

Electron Microscopy of Some Molybdenum Oxide Phases after Use as Catalysts in Oxidative Ammonolysis and Ammoxidation of Toluene

STAFFAN HANSEN* AND ARNE ANDERSSON†

**Department of Inorganic Chemistry 2 and †Department of Chemical Technology, Chemical Center, Lund Institute of Technology, P.O. Box 124, S-221 00 Lund, Sweden*

Received August 17, 1987; in revised form February 4, 1988

Five molybdenum oxide samples, subjected to conditions of oxidative ammonolysis and ammoxidation of toluene at 450 and 460°C, respectively, have been characterized using X-ray diffraction, scanning and transmission electron microscopy, and specific surface area measurements. In oxidative ammonolysis, the relatively large, freshly prepared MoO_3 crystals are reduced to smaller MoO_2 crystals with a crystallite size of 5–30 nm. This process gives a perfectly pseudomorphous product with pores less than 5 nm. The specific surface area increases from $<0.1 \text{ m}^2/\text{g}$ to almost $40 \text{ m}^2/\text{g}$. In subsequent ammoxidation, MoO_2 transforms first into orthorhombic Mo_4O_{11} and finally into MoO_3 . The crystals of Mo_4O_{11} are about $1 \mu\text{m}$ in diameter, and their formation leads to a decrease of specific surface area. The original MoO_3 morphology is retained even after the sequence of transformation as follows: $\text{MoO}_3 \rightarrow \text{MoO}_2 \rightarrow \text{Mo}_4\text{O}_{11} (\rightarrow \text{MoO}_3)$. In some cases, the new generation of MoO_3 crystals grows parallel to the original MoO_3 crystals. © 1988 Academic Press, Inc.

Introduction

Transition metal oxides are widely used as catalysts in selective oxidation of hydrocarbons producing aldehydes, acids, and anhydrides (1). When the oxidation is carried out in the presence of ammonia producing nitrile, the process is called ammoxidation (2). In both cases, oxygen species belonging to the crystal lattice of the catalyst take part in the formation of products (3, 4). The oxygen which has been removed from the crystal surface can then be replaced in a reoxidation process, which involves molecular oxygen. Depending upon the relative rates of oxygen consumption

and catalyst reoxidation, the original catalyst can undergo either reduction or oxidation until steady state is reached (5). The composition at steady state is determined by temperature and partial pressures of reactants. One of the systems which has been extensively characterized, considering structural transformations and defects caused by the influence of gaseous reactants, is the vanadium oxide system used in the ammoxidation of 3-methylpyridine to produce nicotinonitrile (5–9).

Topotactic reactions are important in the preparation of catalytic materials, because they make it possible to control important properties like particle size, crystal habit,

porosity, and specific surface area. For a review, consult the work of Volpe and Boudart (10). These authors state that a toptactic reaction invariably gives a product which is pseudomorphous after the starting material. This is explained by the presence of a structural motif, common to both the starting material and the product. The common structural motif causes an orientational relationship between the two phases and facilitates nucleation of the new phase by acting as a preexisting nucleus. However, it should be noted that even if all toptactic reactions give pseudomorphous products, the reverse relationship is not valid. Pseudomorphs can be formed by many types of nontopotactic reactions or reaction sequences. This is evidenced by many examples from the field of mineralogy. It seems that the creation of a pseudomorph can be likened to the filling of a mold with new material. The only condition put on this new material is that it must form grains which are much smaller than the dimension of the mold itself. The mold, as such, can be a crystal or the impression of a crystal.

Recently, we investigated activities and selectivities of MoO_3 and lower molybdenum oxides, as well as mixtures of molybdenum oxides, in the ammoxidation of toluene to benzonitrile (11). Nitrile was also formed when performing the ammoxidation in absence of gaseous oxygen (11, 12). The latter type of process is known as oxidative ammonolysis (13). As a part of these studies, phase transformations and other solid-state phenomena which occurred through the action of gaseous reactants were characterized by different methods, including scanning and transmission electron microscopy. Here we report the pseudomorphic transformation of MoO_3 into MoO_2 and orthorhombic Mo_4O_{11} as a result of oxidative ammonolysis and ammoxidation of toluene.

Experimental

Preparation of catalysts and catalytic experiments. Crystals of MoO_3 were prepared by sublimation of the powdered chemical (Mallinckrodt, analytical reagent) in a stream of air. The material was then sieved in order to remove the smallest crystals. Lower oxides were obtained by reduction during oxidative ammonolysis of toluene over freshly charged MoO_3 at 450°C . The composition of the reducing stream was toluene 0.78 vol%, ammonia 2.63 vol%, and nitrogen 96.58 vol%. The reduced oxides were also used as catalysts in the ammoxidation of toluene at 460°C , where they became partly reoxidized. In this process, the reactant stream was composed of 0.78 vol% toluene, 2.63 vol% ammonia, 8.78 vol% oxygen, and 87.80 vol% nitrogen. Both the oxidative ammonolysis and the ammoxidation were carried out using a glass reactor. The main products formed were benzonitrile and carbon oxides. After use, the solid samples were rapidly cooled in a nitrogen atmosphere down to ambient temperature and were then transferred, via air atmosphere, to other equipment used for characterization.

Characterization of catalysts. X-ray powder diffractographs were obtained with a Guinier-Hägg camera using $\text{CuK}\alpha_1$ radiation. The interplanar spacings were determined, and the phases present were identified by comparison with the references in the JCPDS file (14). Some oscillation photographs were taken with a Nonius camera utilizing $\text{CuK}\alpha$ X-ray radiation.

Scanning electron micrographs were recorded with a JEOL JSM-T200 instrument. Small amounts of crystals were randomly distributed on a flat holder covered with adhesive tape. A thin layer of gold was then evaporated onto the samples.

Transmission electron micrographs and diffractograms were obtained using a JEOL

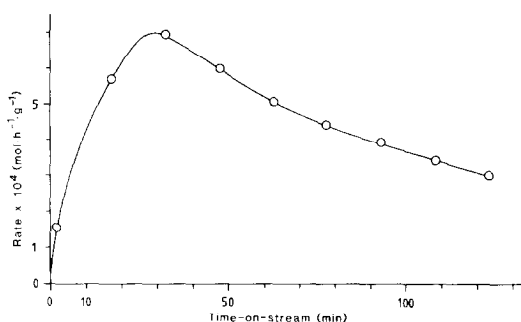


FIG. 1. Total reaction rate of toluene versus time-on-stream for the oxidative ammonolysis.

JEM-200CX microscope. The instrument was operated at an acceleration potential of 200 kV, and the structure image resolution was about 0.23 nm. Specimens were prepared by gentle grinding of crystals suspended in methanol in a small agate mortar. The suspension was then transferred to a copper grid covered with holey carbon film.

Equilibrium N₂ adsorption and desorption isotherms were obtained at 77 K using a gravimetric BET apparatus. Prior to adsorption, the samples were degassed at 300°C for 2 hr at a pressure of 2.7 mPa. The BET surface areas were determined from the adsorption isotherms. For the determinations of pore size distribution, the method of Dollimore and Heal (15) was applied to adsorption isotherms.

Results

Catalytic Tests

Freshly prepared MoO₃ crystals were used as starting material in the oxidative ammonolysis of toluene at 450°C. The formation of products was followed with time-on-stream. Total reaction rate of toluene was calculated and is plotted in Fig. 1. It was observed that the rate per unit mass of MoO₃ at first increased rapidly, then passed through a maximum after which it decreased relatively slowly. This general be-

havior was found to be very reproducible and did not depend on crystal size of the MoO₃ used. However, the position of the maximum shifted toward shorter times when smaller crystals were used. The phase composition of three samples was analyzed by X-ray and electron diffraction. Also the specific surface areas were determined. These results are collected in Table I. Sample 1 is freshly prepared MoO₃. Sample 2 was obtained by running the ammonolysis until maximum activity was achieved, and sample 3 was collected after having carried out the reaction for 2 hr. Samples 2 and 3 were then used as catalysts in the ammoxidation of toluene at 460°C for 1 hr, after which their phase composition (Samples 4 and 5, respectively) were reanalyzed.

From Table I it can be concluded that the initial increase of activity, cf. Fig. 1, is primarily due to the large increase of specific surface area. At activity maximum, the catalyst consists of a mixture of MoO₃ and MoO₂. Prolonged reduction leads to formation of pure MoO₂. Reoxidation of MoO₂ to MoO₃ occurs via Mo₄O₁₁.

Powder Diffraction

Of the many known molybdenum oxides (16, 17), only MoO₃, orthorhombic Mo₄O₁₁, and MoO₂ were identified by X-ray diffrac-

TABLE I
PHASE ANALYSIS AND BET SURFACE AREAS OF
MOLYBDENUM OXIDE SAMPLES

Sample	Treatment	Phases	Surface area (m ² /g)
1	Fresh sample	MoO ₃	<0.1
2	Ammonolysis, activity max.	MoO ₃ , MoO ₂	36.4
3	Ammonolysis, prolonged	MoO ₂	37.8
4	Sample 2 in ammoxidation	MoO ₃ , o-Mo ₄ O ₁₁ (MoO ₃)	1.2
5	Sample 3 in ammoxidation	o-Mo ₄ O ₁₁ (MoO ₃ , MoO ₂)	1.5

TABLE II
CRYSTAL DATA FOR THREE MOLYBDENUM OXIDES

Phase	MoO ₂	Orthorhombic Mo ₄ O ₁₁	Orthorhombic MoO ₃
Color of single cryst.	Reddish brown	Wine red	Pale greenish yellow
Space group	<i>P2₁/c</i> (pseudo <i>P4₂/mnm</i>)	<i>Pnma</i>	<i>Pbnm</i>
Unit cell (Å, °)	<i>a</i> = 5.58 (<i>a</i> = 4.84) <i>b</i> = 4.84 (<i>c</i> = 2.79) <i>c</i> = 5.61 β = 120.9	<i>a</i> = 24.49 <i>b</i> = 5.46 <i>c</i> = 6.75	<i>a</i> = 3.96 <i>b</i> = 13.86 <i>c</i> = 3.70
Point group	<i>2/m</i> (<i>4/mmm</i>)	<i>mmm</i>	<i>mmm</i>
Habit	Nonacicular	Often flat and acicular along [010]	Flat on {010} and elongated along [001]
Density (g/cm ³)	6.53	4.12	4.71

tion of the samples. Some crystal data (16, 18, 19) are presented in Table II.

Orthorhombic Mo₄O₁₁ and MoO₃ gave relatively sharp powder X-ray lines, while the lines of MoO₂ always suffered from extensive broadening. Due to the diffuseness of the MoO₂ lines, no monoclinic splitting was detected, only broadbands corresponding to the tetragonal subcell were observed. This suggests that the coherently scattering domains of this MoO₂ is very small, or somewhere in the range 10–200 nm. Negligible line broadening for Mo₄O₁₁ and MoO₃ indicates crystallites in the range 0.5–10 μ m (20).

Visual Observations

The freshly prepared sample consists of MoO₃ in the form of thin yellowish crystal blades. When these are more or less reduced to MoO₂ by ammonolysis, the color becomes dark reddish brown. No change in the outer appearance of the crystals can be seen by eye, and the crystal surfaces have a high luster. Samples which have undergone ammonolysis followed by amoxidation are dark brown and have a dull luster.

SEM Investigation

The morphology of MoO₃ is illustrated in

Fig. 2a, where four common crystal forms have been included. In addition to these, two more domes (i.e., {*h0l*} forms) and one prism ({*hko*} form) have been described (21). A crystal of normal habit is very thin along [010] and elongated along [001].

A scanning electron micrograph of freshly prepared MoO₃ (Sample 1) is shown in Fig. 2b. The crystals usually have well-developed {100} and {010} faces, while there is a lot of variation in the nature of the terminations in the [001] direction. Many different domes are present, and sometimes the terminations are quite irregular. In certain cases a fishtail shape is observed. This shape would usually be associated with twinning, but in the case of MoO₃ it seems to be a skeletal growth phenomenon. It was observed (Fig. 3) that some crystals have growth steps on the {010} surfaces. These steps are sometimes parallel to a crystal edge. A step height of 0.1 to 1 μ m can be estimated from SEM photographs.

When the catalyst is reduced by ammonolysis, a pseudomorphous replacement of MoO₃ by MoO₂ takes place. A crystal fragment of MoO₃ partially reduced to MoO₂ (Sample 2) is shown in Fig. 4a. No change in the external shape of the crystals or in the smoothness of crystal surfaces can be detected (see Fig. 4b). This behavior does not change even when the crystal is completely transformed into MoO₂ (Sample 3), which is the case in Fig. 5. As could be judged from SEM micrographs, perfect pseudomorphs are formed. Figures 4b and 5b indicate that the size of the MoO₂ grains is less than 0.1 μ m. In addition to an intact MoO₃ morphology, other typical features like {010} surface steps are also preserved (Fig. 6). These steps have a fishtail shape in the *c* direction, though the edges are continuous curves and are not parallel to any crystallographic direction.

A crystal which has been subjected to ammonolysis followed by amoxidation of toluene (Sample 5) is shown in Fig. 7. It has

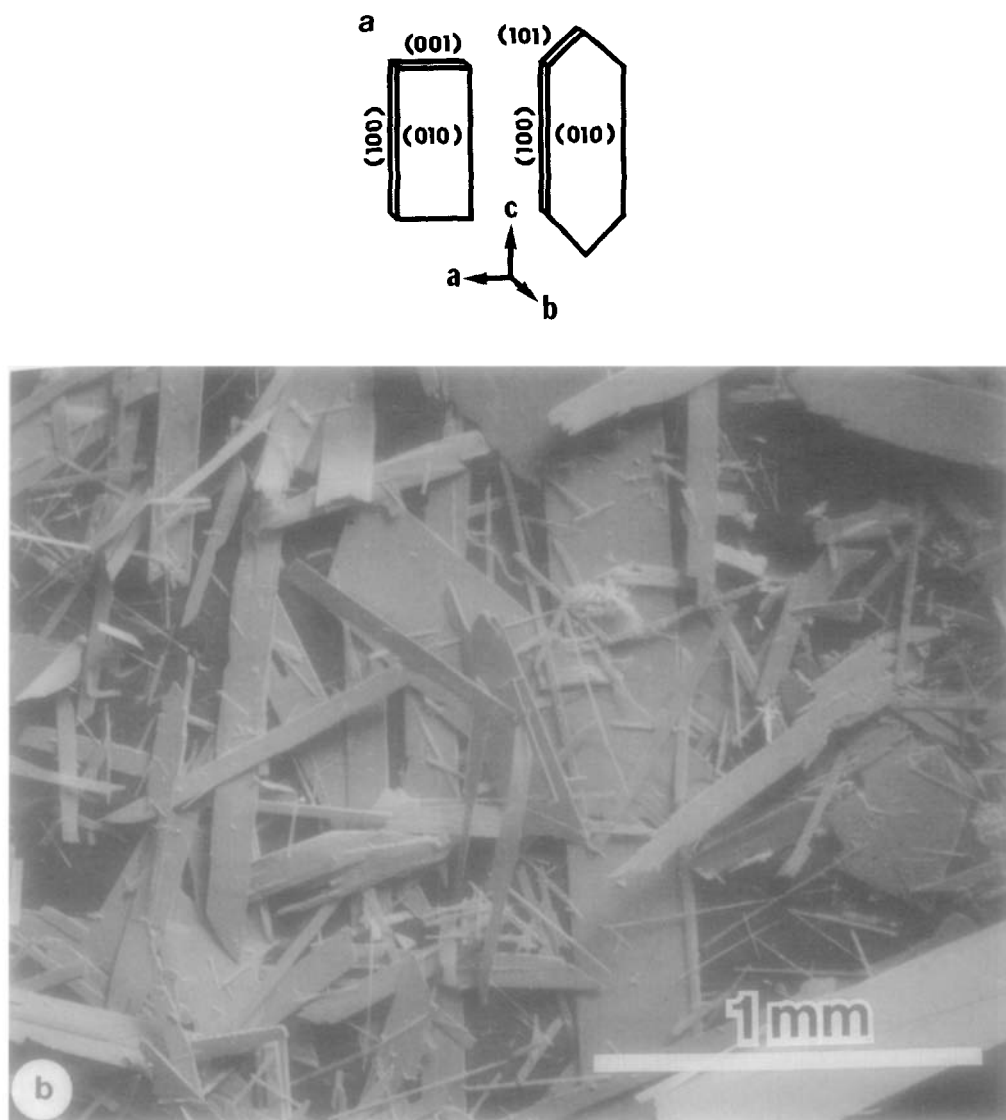


FIG. 2. Orthorhombic MoO_3 . (a) Drawings of idealized crystals. (b) Scanning electron micrograph of MoO_3 prepared by sublimation.

gone through the following sequence of transformation: $\text{MoO}_3 \rightarrow \text{MoO}_2 \rightarrow \text{Mo}_4\text{O}_{11}$. Despite one additional reaction step, the original crystal morphology of MoO_3 has not been greatly affected. The equant Mo_4O_{11} crystals are randomly oriented, and their size is $0.1\text{--}2\ \mu\text{m}$. There is a difference between the habit of the crystals in Fig. 7b

and the habit described in the literature (Table II). However, since this sample only contains trace amounts of other phases, there is little doubt about the identity of the crystals.

A comparatively complex crystal texture is observed for crystals that have been subjected to reduction during a shorter period

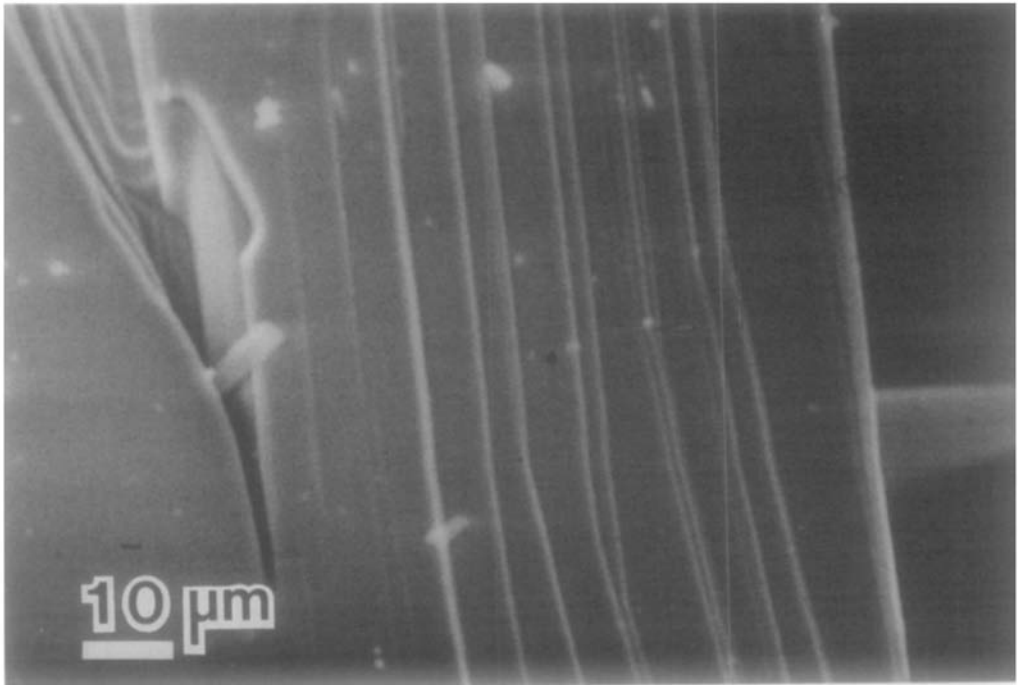


FIG. 3. SEM photograph of growth steps on the (010) surface of a MoO_3 crystal.

of time before they were used in ammoxidation (Sample 4). After the period of ammoxidation, they consist of MoO_3 and MoO_2 . During subsequent ammoxidation, a transformation takes place in the order: $\text{MoO}_2 \rightarrow \text{Mo}_4\text{O}_{11} \rightarrow \text{MoO}_3$. In Fig. 8a some crystals from this sample are shown. The typical MoO_3 habit is still visible, but below the coarse surface, a new generation of flat crystals can be noticed. In an enlarged micrograph (Fig. 8b, by comparison with Fig. 7b), the surface layer can be identified as Mo_4O_{11} . The tabular crystals beneath the Mo_4O_{11} crystals are identified as MoO_3 by their morphology. Crystal morphology also indicates that the original MoO_3 crystal and the new generation of MoO_3 tablets have exactly the same orientation. Some textural variations can be noticed in the phase on top of the well-crystallized layer of MoO_3 . Comparison of Figs. 8 and 9 shows that the top layer of the specimen in Fig. 9 is of

much finer grains. In some areas the surface is compact, while in other parts there is a network of ridges.

TEM Investigation

A micrograph of a multiphase sample (Sample 4) is shown in Fig. 10. The grain marked A was identified by selected area diffraction as a single crystal of Mo_4O_{11} , while the thin blade marked B is a MoO_3 crystal of normal habit. Thin blades can thus be assumed to be MoO_3 , while thicker grains are presumably Mo_4O_{11} . All particles have dimensions of about $0.5 \mu\text{m}$. These observations support the identification of phases in Fig. 8b.

From transmission electron micrographs it becomes clear why the MoO_2 pseudomorphs after MoO_3 (Sample 3) are microporous (see Fig. 11a). Each single crystal of MoO_3 is transformed into a large number of MoO_2 microcrystals with a size of only 5 to

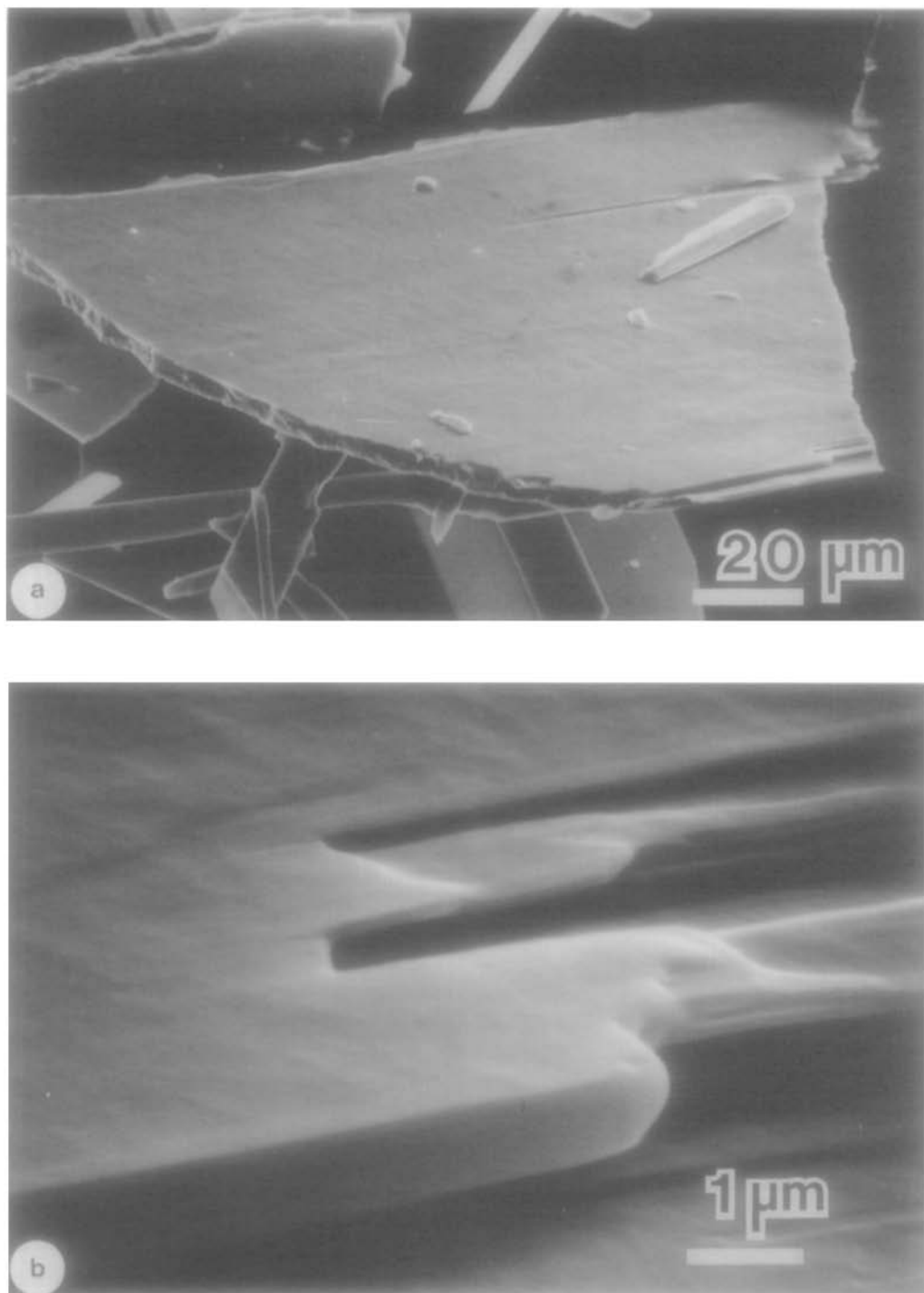


FIG. 4. SEM photograph of MoO_3 partly reduced to MoO_2 . (a) Fragment of a broken crystal. (b) Enlargement of the lower right corner of the previous figure, showing smooth (010) and (100) faces.

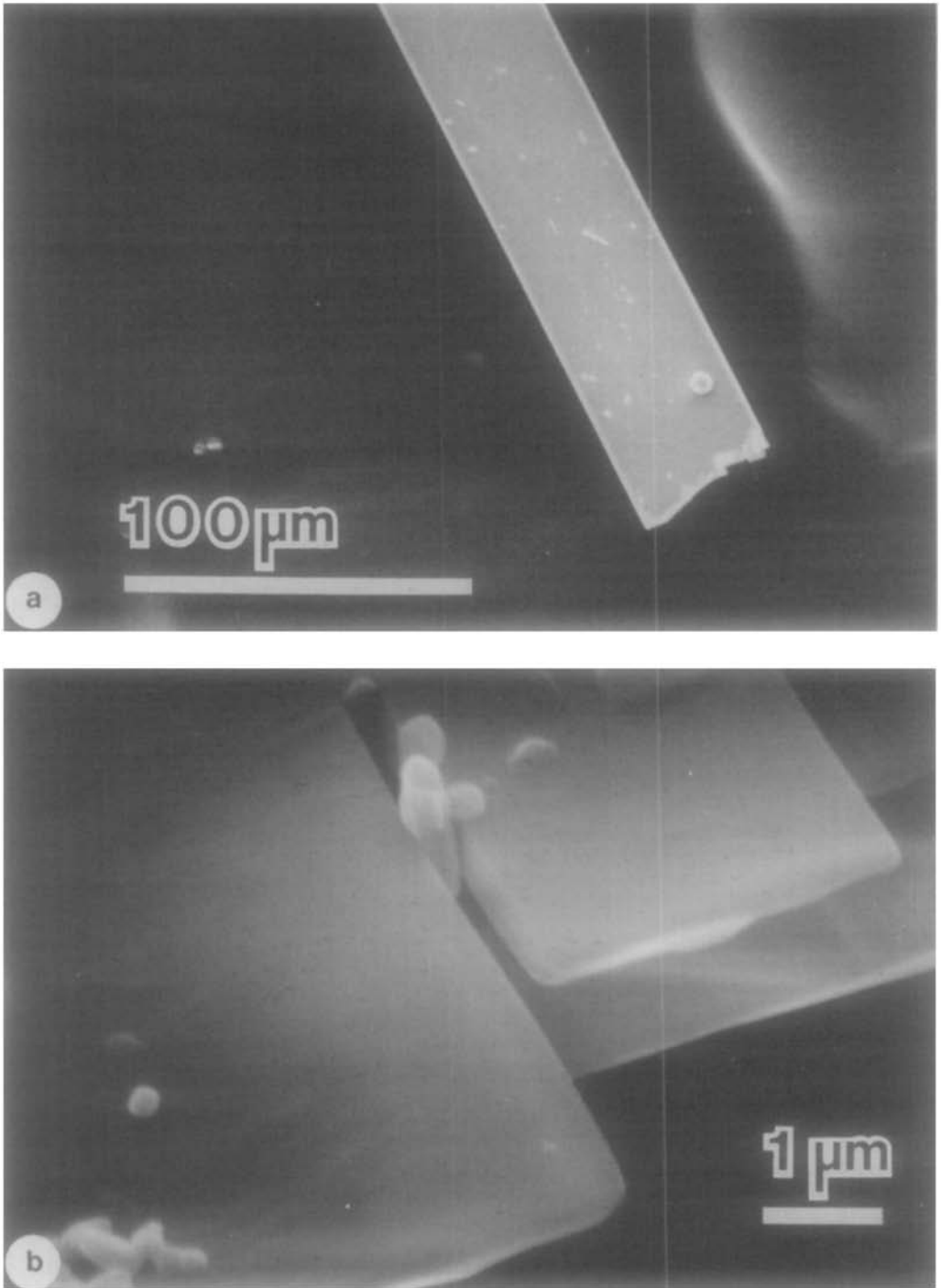


FIG. 5. Scanning electron micrographs of a MoO_3 crystal which has been completely reduced to MoO_2 . (a) Pseudomorph showing the original MoO_3 habit. (b) Blow up of the lower right corner, exhibiting the (100), (010), and (001) faces of MoO_3 .

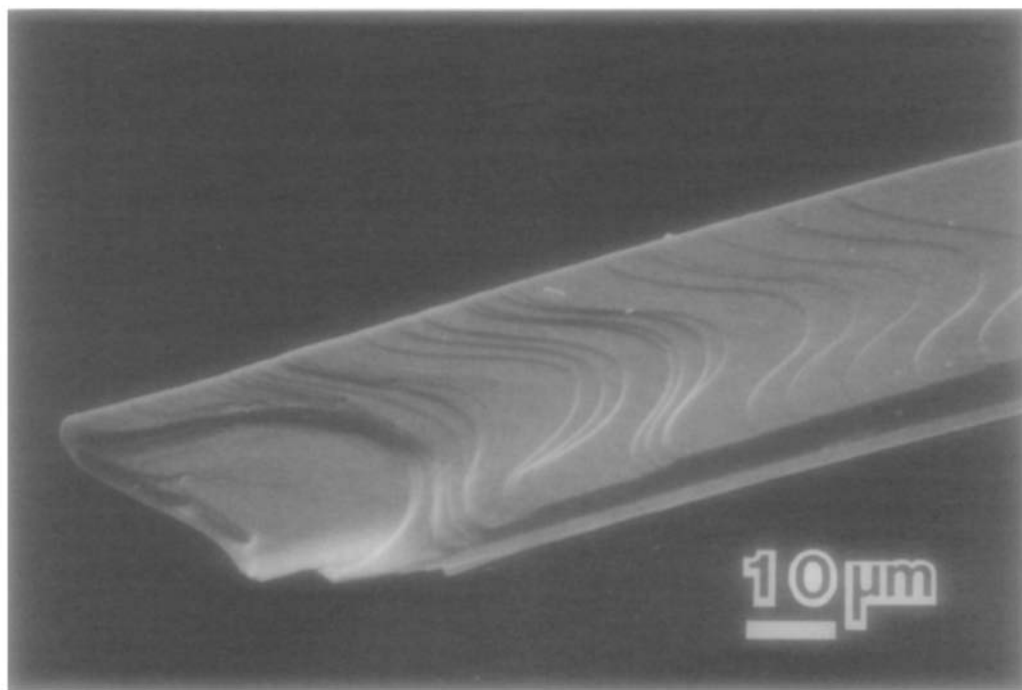


FIG. 6. Scanning electron micrograph of a MoO_2 pseudomorph after MoO_3 displaying steps on the former MoO_3 (010) surface (c.f. Fig. 3).

30 nm. The dimension of the pores is difficult to measure directly from the micrograph, since it is inherent in the method of transmission electron microscopy that a projection of the object is obtained. In spite of this, the image implies that the dimensions of the pores should be smaller than the dimensions of the individual crystals, since these appear to be fairly close packed. That each grain in Fig. 11a is a single crystal of MoO_2 is evident from the image in Fig. 11b. At the surface of the crystals, small steps can be seen. These have a height of a few tenths of a nanometer and correspond to steps consisting of a few atoms.

Lattice images often show that a group of microcrystals have the same orientation. This is also borne out by the fact that aggregates of microcrystals give a single crystal type of diffraction pattern, usually with

[111] or [001] as the zone axis in the pseudotetragonal setting for MoO_2 . This suggests the possibility of a topotactic reaction, an idea which was tested by means of oscillation photographs of a MoO_2 pseudomorph after MoO_3 (Sample 3). A well-formed thin plate, about $0.4 \times 0.01 \times 0.7$ mm, was mounted with the [010] direction of MoO_3 along the camera axis. The films displayed powder rings from MoO_2 without indication of a preferred orientation.

Adsorption Isotherms and Pore Size Distributions

Complete N_2 adsorption-desorption isotherms at equilibrium relative pressures in the range 0.013–0.985 were recorded for the two samples having the largest BET surface areas (Samples 2 and 3). Figure 12 presents the isotherms for Sample 2. The type of isotherms was found to be identical

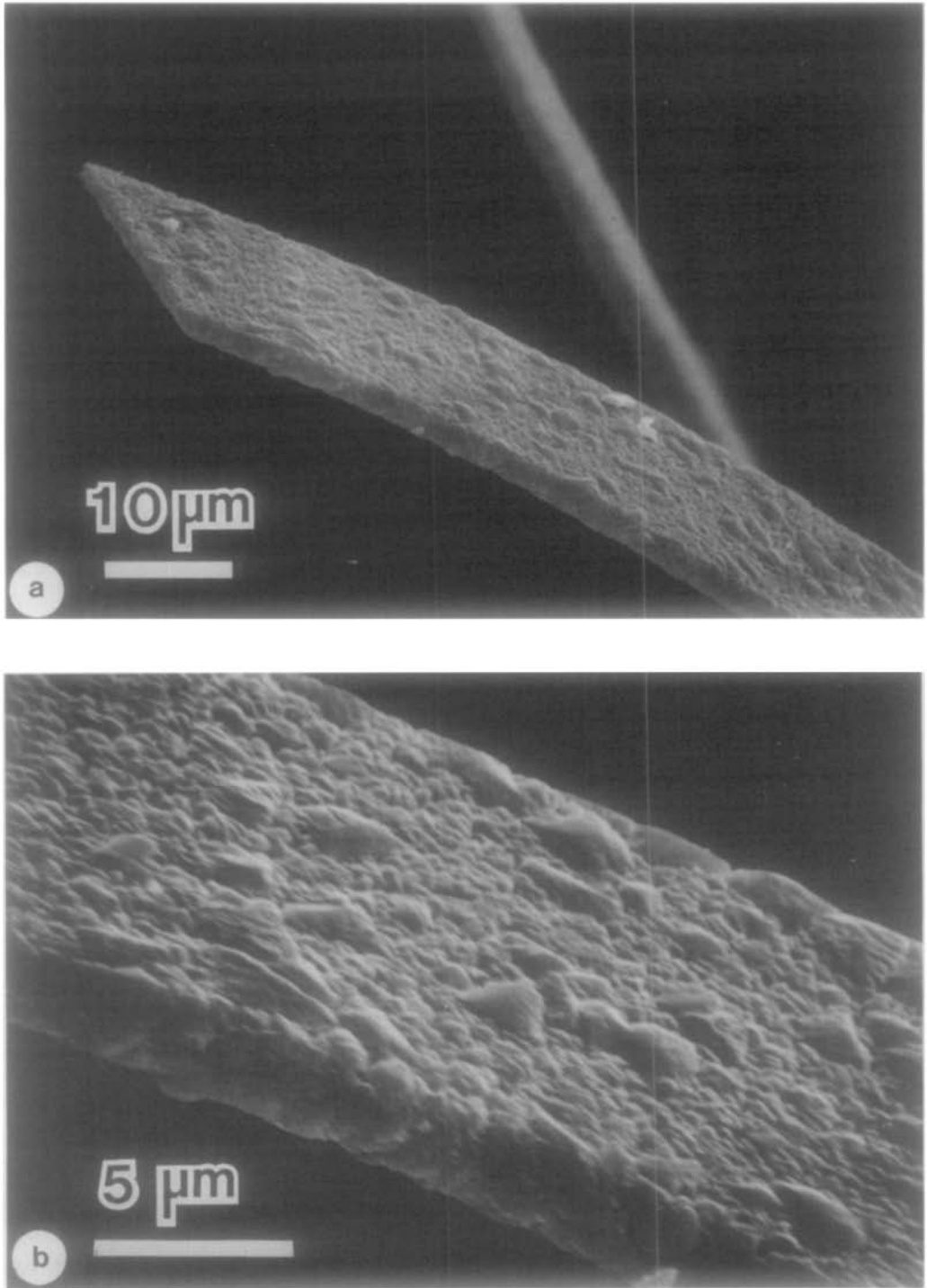


FIG. 7. SEM photos of a polycrystal consisting mainly of orthorhombic Mo_4O_{11} . (a) The original MoO_3 habit is still visible. (b) Enlargement showing blocky Mo_4O_{11} crystals in random orientation.

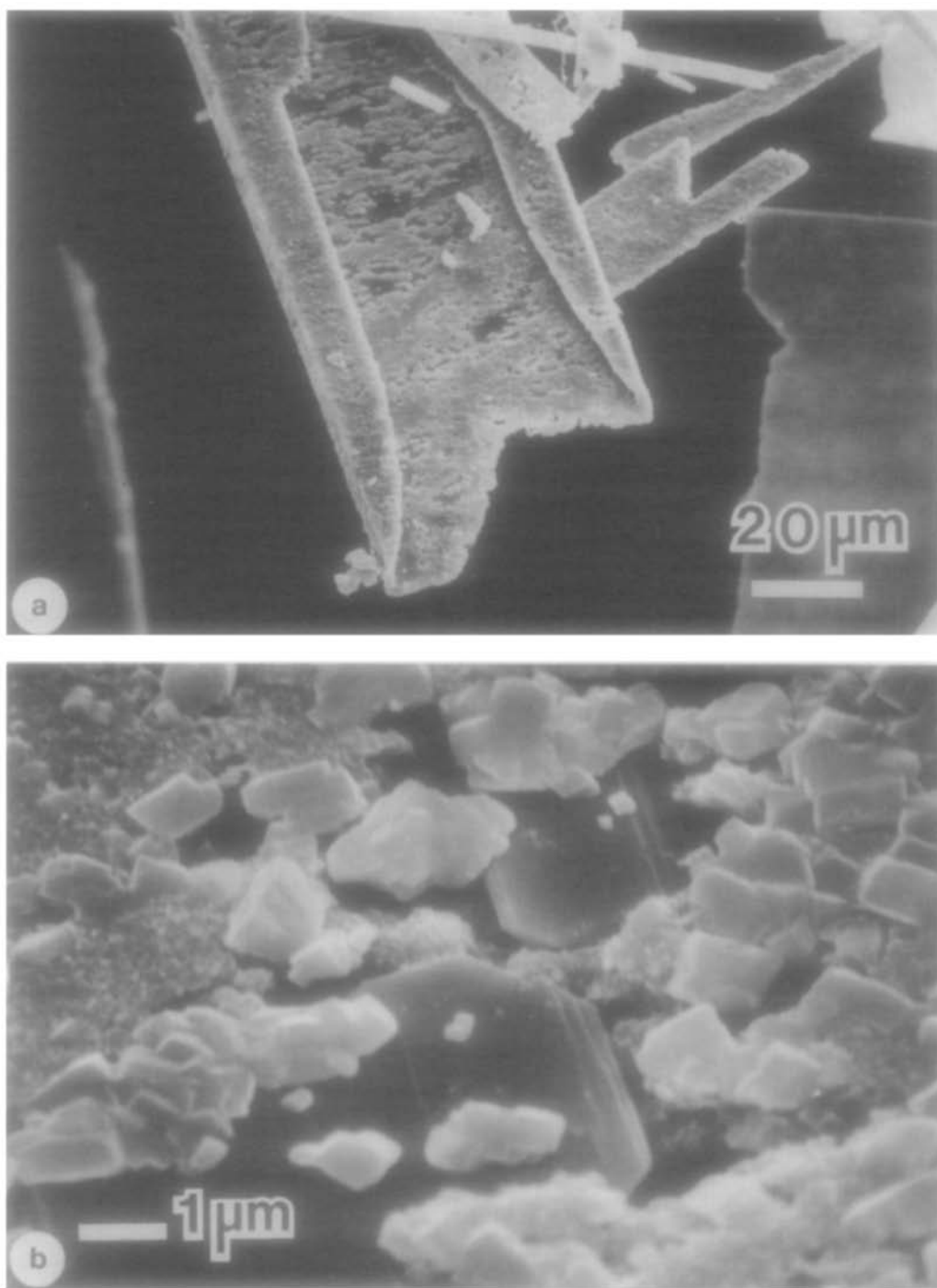


FIG. 8. Scanning micrographs of a sample containing mainly orthorhombic Mo_4O_{11} and MoO_3 phases. (a) Pseudomorphic fish-tail habit. (b) Detail showing small, randomly oriented crystals of Mo_4O_{11} and well-formed and well-oriented MoO_3 tablets below the Mo_4O_{11} layer. Note the parallel crystal edges in the two figures.

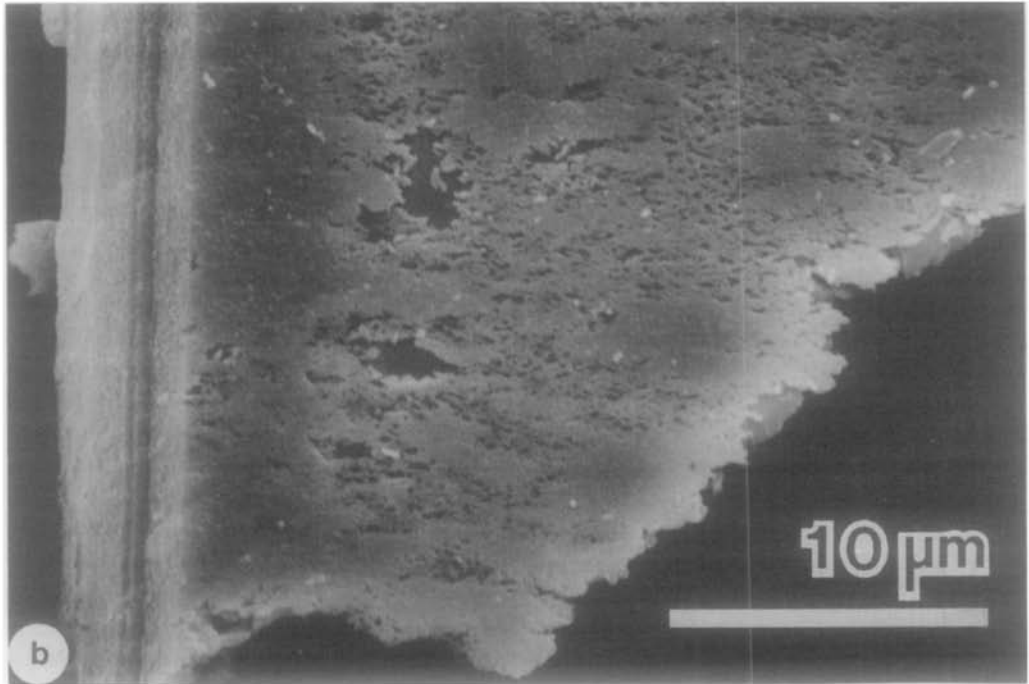
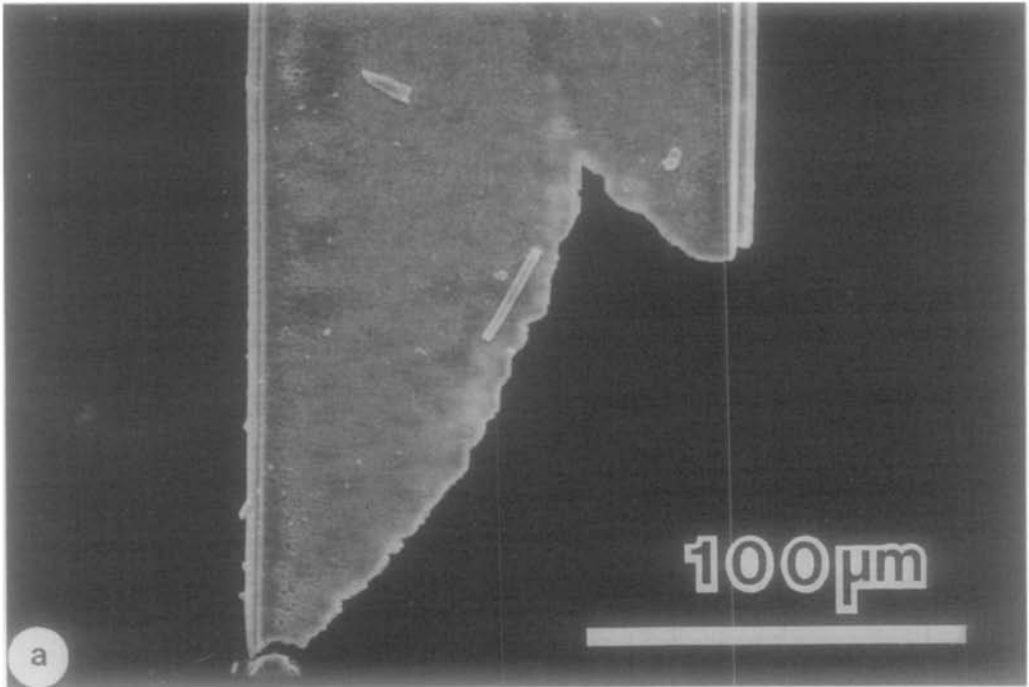


FIG. 9. SEM photographs of a $\text{MoO}_3/\text{Mo}_4\text{O}_{11}$ sample. (a) Crystal with typical MoO_3 habit and a surface layer of varying texture. (b) Layer of MoO_3 crystals situated beneath the phase covering the surface. Best seen at the edge to the right. (c) Fine grained surface phase, dense to the right and forming a ridge pattern to the left. The ridges show a preferred orientation approximately along the two diagonals of the photograph.

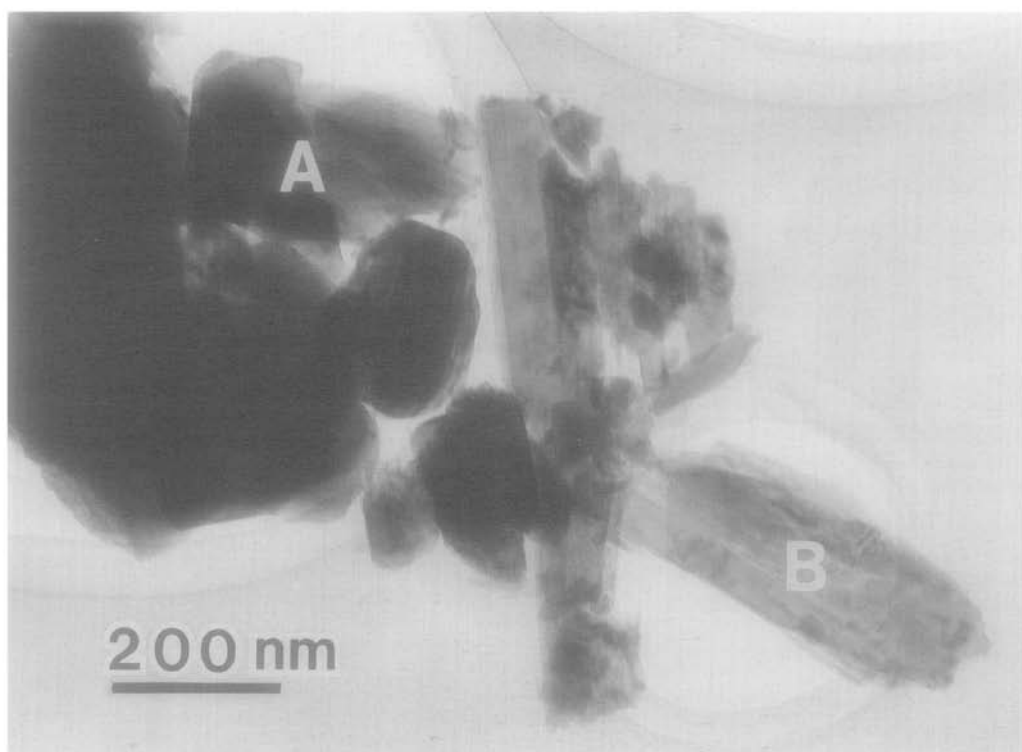
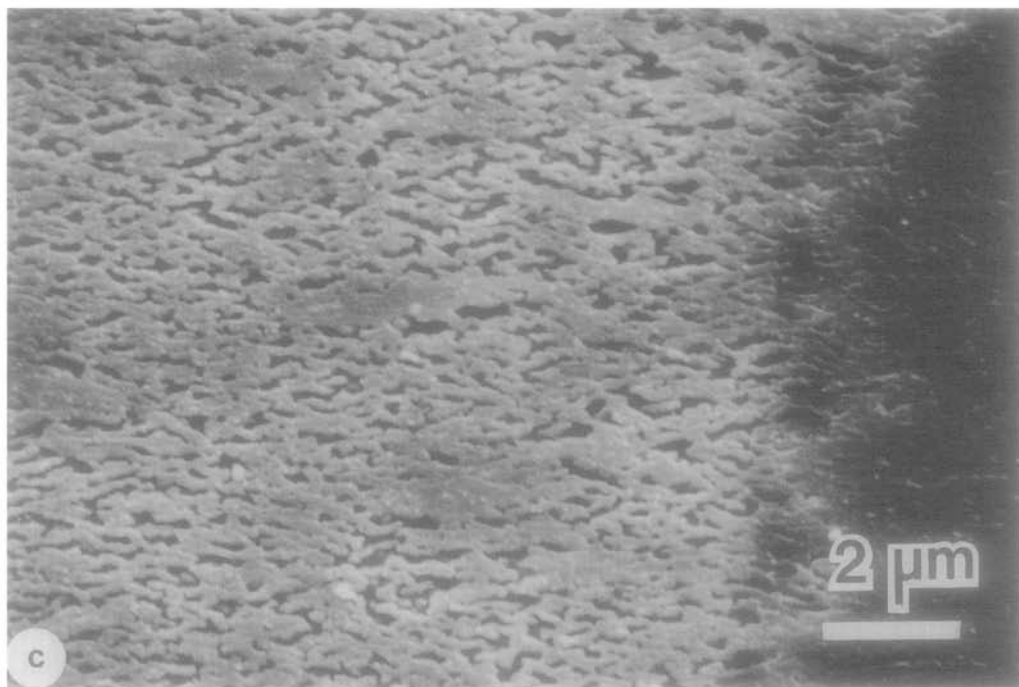


FIG. 10. Transmission electron micrograph of a sample containing thin MoO_3 crystals and thicker crystals of orthorhombic Mo_4O_{11} . (A) A Mo_4O_{11} crystal with $[100]$ along the beam; (B) a MoO_3 crystal flattened on $\{010\}$.

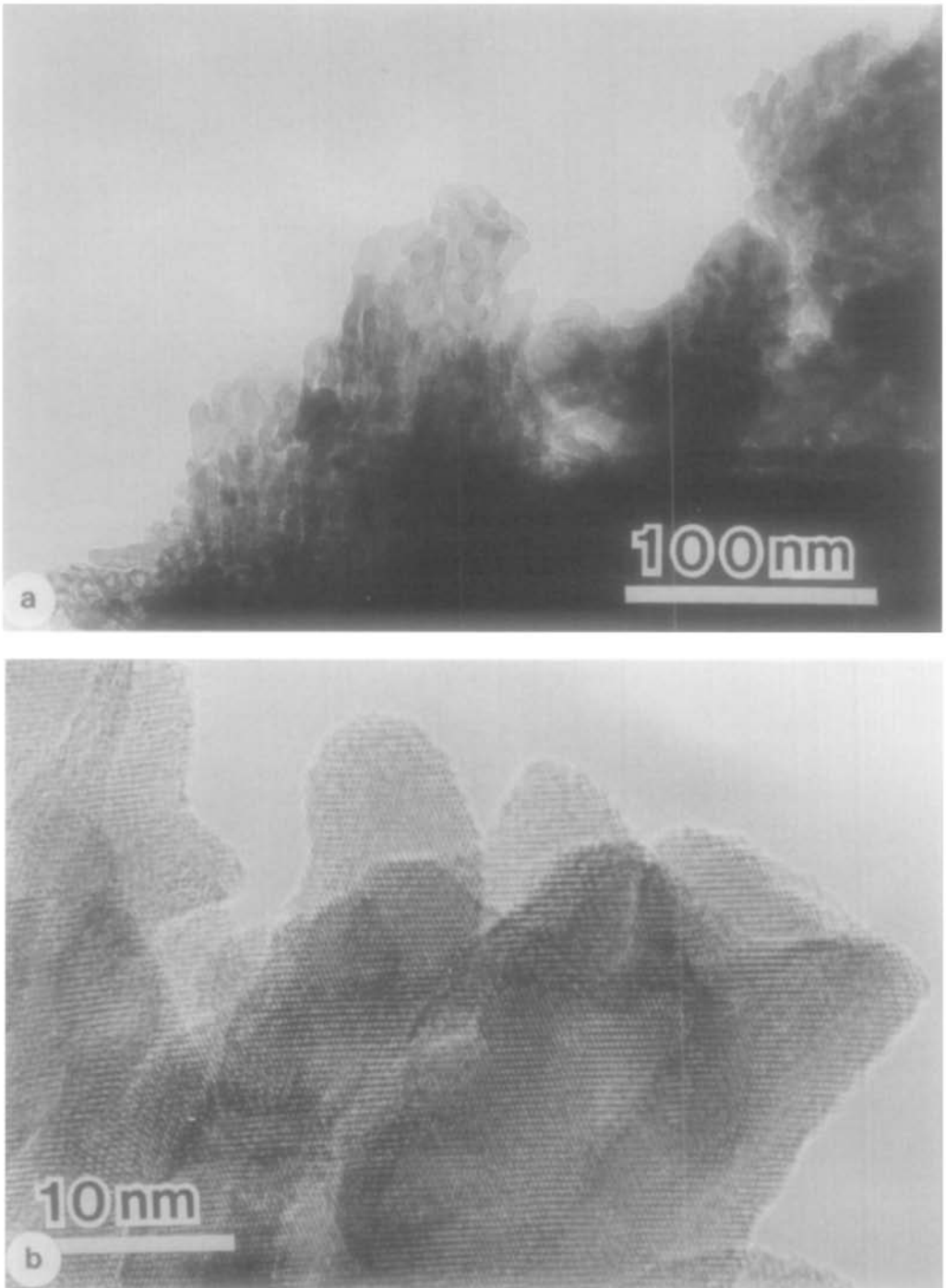


FIG. 11. TEM images of a MoO_2 pseudomorph after MoO_3 . (a) Microporous solid consisting of small MoO_2 crystallites. (b) High-resolution image of MoO_2 microcrystals with the pseudotetragonal $[111]$ direction along the electron beam.

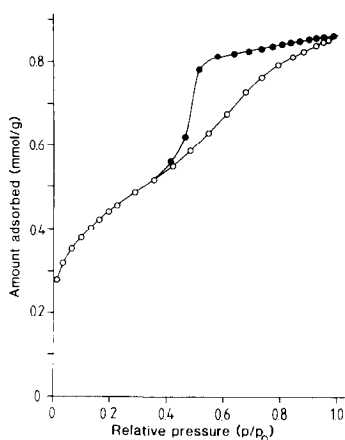


FIG. 12. Equilibrium N_2 adsorption (○)–desorption (●) isotherms for Sample 2 (MoO_3/MoO_2) at 77 K. Monolayer capacity 0.46 mmol/g.

for both samples and can be described as a combination of Type I and IV isotherms (22). The relatively steep increase at $p/p_0 < 0.01$ is typical for Type I isotherms and may partly be due to filling of micropores (< 2 nm) whose uptake is controlled by the accessible volume rather than by the internal surface area. However, the BET plots were found to be linear in the range $0.035 < p/p_0 < 0.220$. No distinct sharp increase in the adsorption isotherms was noticed at high relative pressures. Thus, it can be sug-

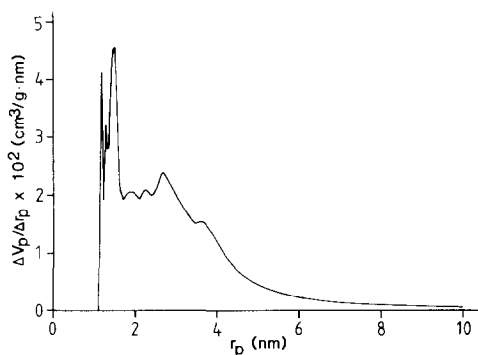


FIG. 13. Pore size distribution for Sample 2 (MoO_3/MoO_2). V_p , pore volume per unit mass of adsorbent; r_p , pore radius.

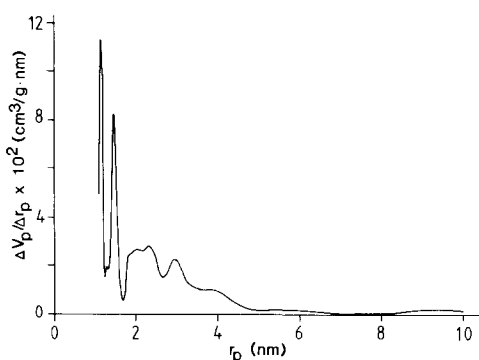


FIG. 14. Pore size distribution for Sample 3 (MoO_2).

gested that the multilayer adsorption is accompanied by capillary condensation in mesopores having a rather wide pore size distribution.

In calculations of pore size distributions, usually the desorption branch of the isotherm is used. However, for Samples 2 and 3 the hysteresis loop is of H2 type, formerly termed Type E. For such a case it is recommended that the adsorption branch should be used (22). The pore size distributions of Samples 2 and 3 are given in Figs. 13 and 14, respectively. Considering these figures, it is obvious that most pores have radii which are less than 5 nm. From the uptake of liquid nitrogen, the pore volume was determined to be 0.030 and 0.029 cm^3/g for Samples 2 and 3, respectively.

Discussion

Several solid oxide phases exist in which Mo has an average oxidation state in the range +4 to +6. Structural features of phases existing between 500 and 800°C in the MoO_2 – MoO_3 system have been investigated and summarized by Kihlborg (16, 17). The following phases were included: MoO_2 (18), orthorhombic Mo_4O_{11} ($MoO_{2.750}$, stable above 615°C), monoclinic Mo_4O_{11} (stable below 615°C), $Mo_{17}O_{47}$ ($MoO_{2.765}$), Mo_5O_{14} ($MoO_{2.800}$, metastable?), Mo_8O_{23} ($MoO_{2.875}$), triclinic $Mo_{18}O_{52}$ ($MoO_{2.889}$,

stable below 740°C), monoclinic Mo_9O_{26} ($\text{MoO}_{2.889}$, stable above 740°C), and orthorhombic MoO_3 . A metastable monoclinic (pseudo-hexagonal) polymorph of MoO_3 is also known (23). Structurally, the molybdenum oxides can be classified as follows: (i) MoO_2 has a rutile structure with monoclinic distortion; (ii) MoO_3 adopts a unique type of layer structure, while triclinic $\text{Mo}_{18}\text{O}_{52}$ has a shear structure based on this structure; (iii) the two forms of Mo_4O_{11} , as well as Mo_8O_{23} and Mo_9O_{26} , contain slabs of the ReO_3 structure type; (iv) $\text{Mo}_{17}\text{O}_{47}$ and Mo_5O_{14} have structures somewhat similar to the tungsten bronzes with MoO_6 octahedra and MoO_7 bipyramids (16, 17).

Things are further complicated by the existence of at least one series of homologous structures generated by a shear mechanism. The structure of $\text{Mo}_{18}\text{O}_{52}$ was determined by Kihlberg (24), who suggested that this was one member of a series of shear structures based on the MoO_3 structure and with a general formula of $\text{Mo}_n\text{O}_{3n-m+1}$, where n is related to the thickness of the slabs, and m determines the direction of the shear planes. In this series, $\text{Mo}_{18}\text{O}_{52}$ is the member with $n = 18$ and $m = 3$. X-ray diffraction data also indicated the presence of $\text{Mo}_{13}\text{O}_{38}$ ($n = 13$, $m = 2$) and $\text{Mo}_{26}\text{O}_{75}$ ($n = 26$, $m = 4$) (24). Bursill (25), using electron optical methods, later identified additional phases ($n = 19-22$, $m = 3$) belonging to this series. Based on other parent structures, three additional homologous series have been postulated (19, 26), but have so far not been observed. Relevant in this context also is the possible formation of hydroxyl-containing compounds (27), e.g., $\text{Mo}_4\text{O}_{10}(\text{OH}_2)$ (28), which has a crystal structure very similar to that of orthorhombic MoO_3 (29).

In view of the many existing molybdenum oxides, it is somewhat surprising that in the present study only three of these were identified by powder X-ray diffraction, i.e., MoO_2 , orthorhombic Mo_4O_{11} ,

and MoO_3 . The reason is not obvious; although, first of all our system is not a simple Mo-O system, and second, the reactions may be determined by kinetic factors. If the latter is the case, then it may be relevant that the phases formed are the three phases which are stable at the highest temperatures (30) (cf. Ostwald's rule). *In situ* reduction of MoO_3 in a transmission electron microscope was studied by Bursill (31). Depending on the intensity of the electron beam, the final product was either orthorhombic Mo_4O_{11} or MoO_2 . Another interesting observation concerns the rate of oxidation. It has been found that MoO_2 , in air at about 300°C, is oxidized very slowly, while orthorhombic Mo_4O_{11} is the molybdenum oxide which is most readily oxidized (30). This can explain why traces of MoO_2 were present in Samples 4 and 5.

Reduction of MoO_3 or ammonium molybdate to MoO_2 with hydrogen at about 550°C is the first step in industrial production of Mo metal (32). MoO_2 is then reduced to metal by hydrogen at about 1100°C. Carpenter and Hallada (32) showed that the habit of resulting MoO_2 particles depends on whether ammonia is present in the first reduction step. The shape obtained is then retained when metal powder is produced, thus giving powders with different properties in subsequent compressing and sintering steps. In the presence of ammonia, equidimensional MoO_2 crystals are formed, while reduction with hydrogen gives lath-like particles. The dimension of the particles are, in both cases, in the order of 1 μm . The habit of the MoO_2 crystals obtained in the present investigation is equidimensional or slightly elongated, but they are much smaller, about 0.01 μm . It is not clear whether the lath-like MoO_2 particles observed by Carpenter and Hallada (32) were single crystals of MoO_2 , or MoO_2 pseudomorphs after lath-like MoO_3 crystals.

Bertrand and Dufour (33, 34) observed that reduction in hydrogen at 450-470°C of

millimeter-sized MoO_3 crystals gives pseudomorphs consisting of micrometer-sized MoO_2 crystal laths. These are crystallographically well-oriented relative to the original MoO_3 crystal, i.e., the reaction is topotactic. Another example of a reaction, which is both topotactic and pseudomorphic, is the transformation of MoO_3 crystals to $\gamma\text{-Mo}_2\text{N}$ in a stream of pure ammonia at atmospheric pressure and at a temperature being increased from 360 to 710°C (35). The morphology of the MoO_3 crystals is perfectly preserved, since the average size of the $\gamma\text{-Mo}_2\text{N}$ crystals is only 3 nm, as they are estimated from a specific surface area value of 220 m^2/g . The present investigation shows a pseudomorphic transformation of MoO_3 to MoO_2 , coupled with a drastic increase in specific surface area. More work on specimens containing both oxides is needed in order to definitely determine whether this is a topotactic reaction. Even after reoxidation of MoO_2 to orthorhombic Mo_4O_{11} , the MoO_3 morphology is kept intact, although the Mo_4O_{11} crystals have now reached a size which gives the pseudomorphs a dull luster. On the other hand, the pseudomorphs formed in the initial reduction process have a high luster, due to the small size of the MoO_2 crystallites.

Obtaining an average value of crystal size should in principle be possible both from micrographs and from specific surface area measurements. From scanning electron micrographs of Samples 4 and 5, e.g., Figs. 7 and 8, the particle size of the Mo_4O_{11} crystals can be estimated to be of the order 0.1–2 μm . If the crystals are assumed to have the shape of small cubes, then the crystal edge (d) can be calculated according to

$$d = 6/(S \times \rho), \quad (1)$$

where S and ρ are specific surface area and crystal density, respectively. Combining values on specific surface areas (Table I) with values on crystal densities (Table II)

the average particle size can be calculated to be 1.1 and 1.0 μm for Samples 4 and 5, respectively. These values agree very well with those estimated from micrographs.

When MoO_3 was reduced to MoO_2 in oxidative ammonolysis, the specific surface area increased from about 0.1 to almost 40 m^2/g . No Mo_2N was found to be formed, which was reported to be the case when MoO_3 was reacted with pure ammonia (35). In that case the surface area increased even more, up to 220 m^2/g . Reduction of MoO_3 to MoO_2 leads to a decrease of the unit cell volume per Mo atom. However, considering scanning electron micrographs, the external shape of the original crystals was retained. There were no indications of any shrinkage, which means that a porous material must be formed. Then by the use of crystal density values (Table II) in combination with the experimentally determined value of specific pore volume, 0.030 cm^3/g , the composition of Sample 2 can be calculated to be 62 mole% MoO_3 and 38 mole% MoO_2 , on the condition that all pores are open. Such a composition is not contradictory to observed intensities of X-ray lines. These indicated that the amounts of both oxides were of the same magnitude. If the core of each polycrystal of Sample 2 consists of a single crystal of MoO_3 surrounded by a large number of MoO_2 microcrystals, then it is reasonable to assume that the total specific surface area of the sample is mainly determined by the area of the MoO_2 crystals. Using the value of the composition calculated above, the specific surface area of the MoO_2 fraction can be estimated to be 104 m^2/g , which according to Eq. (1) corresponds to a particle size of 9 nm. This value is within the range, 5–30 nm, that could be determined from transmission electron micrographs.

The pore volume of Sample 3 was determined to be 0.029 cm^3/g . On the condition that the solid's exterior is retained, the theoretically calculated value is 0.086 cm^3/g .

Thus, it seems that prolonged reduction of MoO_3 gives porous MoO_2 with a large fraction of its pores being closed. Formation of blocked pores was also observed in the transformation of MoO_3 to Mo_2N (35). A rough estimate of particle size can be obtained if it is assumed that closed and open pores are of the same size and shape. In such a case, the actual void area is measured specific surface area \times theoretical pore volume/measured pore volume, i.e., $(37.8 \times 0.086/0.029) = 112 \text{ m}^2/\text{g}$. From Eq. (1) the average particle size can be calculated to be 8 nm. This value is almost identical to that calculated for Sample 2, which agrees with the results of TEM showing that the MoO_2 microcrystals in Samples 2 and 3 were of the same size.

Sample 4 displays some interesting textural features. Considering Figs. 8b and 9b, a new generation of MoO_3 crystals with smooth surfaces can be seen below the top layer of small orthorhombic Mo_4O_{11} crystals. This new generation is parallel to the original MoO_3 crystal, a fact which can be explained if it is assumed that after reduction the periphery of the crystal consists of MoO_2 , while unreacted MoO_3 remains in the center of the crystal. In the subsequent oxidation process, the outer layer of MoO_2 is first transformed into Mo_4O_{11} , and then into MoO_3 . When the new generation of MoO_3 crystals is formed, the original MoO_3 crystal in the center act as a nucleation site, and new crystals grow on the remains of the old crystal. It is also possible that some recrystallization of the original MoO_3 crystal takes place.

The ridge pattern formed in some parts of the top layer of the crystal in Fig. 9 could be a textural remnant of the typical cross-hatched patterns which are formed on $\{010\}$ MoO_3 by a slight reduction of the surface layer (31, 35–38). Several models have been proposed for these domains (27, 31, 34), which give rise to diffuse scattering in electron diffraction patterns. A striking

similarity can be observed between Fig. 9c and the grating used in Ref. (39) to simulate these diffuse scattering effects. However, a problem is that the c -axis bisects the obtuse angle formed by the two directions of ridges in Fig. 9c, while on the contrary, the c -axis is reported to bisect the acute angle formed by the two main directions of the surface domain patterns on slightly reduced MoO_3 crystals (31, 36–38). The direction of the c -axis has been inferred from the general habit of the crystal, since the quality of the terminating faces of the crystal in Fig. 9 does not allow a conclusive measurement of interfacial angles (cf. Fig. 2a). One possible explanation for the discrepancy is that, on rare occasions, crystals elongated along the a -axis are formed.

Acknowledgment

The authors gratefully acknowledge financial support from the National Swedish Board for Technical Development (STU).

References

1. K. WEISSERMEL AND H.-J. ARPE, "Industrial Organic Chemistry," Verlag Chemie, Weinheim (1978).
2. R. K. GRASSELLI AND J. D. BURREINGTON, in "Advances in Catalysis" (D. D. Eley, H. Pines, and P. B. Weisz, Eds.), Vol. 30, pp. 133–163, Academic Press, New York (1981).
3. J. HABER, in "Solid State Chemistry in Catalysis" (R. K. Grasselli and J. F. Brazdil, Eds.), ACS Symposium Series, Vol. 279, pp. 3–21, Amer. Chem. Soc., Washington, DC (1985).
4. R. K. GRASSELLI, J. F. BRAZDIL, AND J. D. BURREINGTON, in "Proceedings, International Congress on Catalysis, 8th (Berlin 1984)," Vol. V, pp. 369–380, Verlag Chemie, Weinheim (1984).
5. A. ANDERSSON, *J. Catal.* **69**, 465 (1981).
6. A. ANDERSSON AND S. T. LUNDIN, *J. Catal.* **58**, 383 (1979).
7. A. ANDERSSON, R. WALLENBERG, S. T. LUNDIN, AND J.-O. BOVIN, in "Proceedings, International Congress on Catalysis, 8th (Berlin 1984)," Vol. V, pp. 381–392, Verlag Chemie, Weinheim" (1984).
8. A. ANDERSSON AND J.-O. BOVIN, *Naturwissenschaften* **72**, 209 (1985).

9. A. ANDERSSON, J.-O. BOVIN, AND P. WALTER, *J. Catal.* **98**, 204 (1986).
10. L. VOLPE AND M. BOUDART, *Catal. Rev. Sci. Eng.* **27**, 515 (1985).
11. A. ANDERSSON AND S. HANSEN, to be submitted for publication.
12. A. ANDERSSON AND S. HANSEN, submitted for publication.
13. M. C. SZE AND A. P. GELBEIN, *Hydrocarbon Process.* **55**(2), 103 (1976).
14. "Powder Diffraction File," JCPDS International Centre for Diffraction Data, Swarthmore (1985).
15. D. DOLLIMORE AND G. R. HEAL, *J. Appl. Chem.* **14**, 109 (1964).
16. L. KIHILBORG, *Ark. Kemi* **21**, 471 (1964).
17. L. KIHILBORG, *Adv. Chem. Ser.* **39**, 37 (1963).
18. A. MAGNÉLI AND G. ANDERSSON, *Acta Chem. Scand.* **9**, 1378 (1955).
19. L. KIHILBORG, *Ark. Kemi* **21**, 365 (1963).
20. L. V. AZAROFF AND M. J. BUERGER, "The Powder Method in X-Ray Crystallography," p. 255, McGraw-Hill, New York (1958).
21. A. E. NORDENSKJÖLD, *Poggendorff's Ann. Phys. Chem.* **112**, 160 (1861).
22. K. S. W. SING, D. H. EVERETT, R. A. W. HAUL, L. MOSCOU, R. A. PIEROTTI, J. ROUQUÉROL, AND T. SIEMIENIEWSKA, *Pure Appl. Chem.* **57**, 603 (1985).
23. E. YODA, *J. Phys. Soc. Japan* **15**, 821 (1960).
24. L. KIHILBORG, *Ark. Kemi* **21**, 443 (1964).
25. L. A. BURSILL, *Acta Crystallogr. Sect. A* **28**, 187 (1972).
26. A. MAGNÉLI, *Acta Crystallogr.* **6**, 495 (1953).
27. L. A. BURSILL, W. C. T. DOWELL, P. GOODMAN, AND N. TATE, *Acta Crystallogr. Sect. A* **34**, 296 (1978).
28. K.-A. WILHELMI, *Acta Chem. Scand.* **23**, 419 (1969).
29. L. KIHILBORG, *Ark. Kemi* **21**, 357 (1963).
30. L. KIHILBORG, *Acta Chem. Scand.* **13**, 954 (1959).
31. L. A. BURSILL, *Proc. R. Soc. London Ser. A* **311**, 267 (1969).
32. K. H. CARPENTER AND C. J. HALLADA, in "Proceedings, Climax 3rd International Conference on the Chemistry and Uses of Molybdenum" (H. F. Barry and P. C. H. Mitchell, Eds.), pp. 204-208, Climax Molybdenum Co., Ann Arbor (1979).
33. O. BERTRAND AND L.-C. DUFOUR, *C.R. Acad. Sci. Paris Ser. C* **278**, 315 (1974).
34. O. BERTRAND AND L.-C. DUFOUR, *Phys. Status Solidi A* **60**, 507 (1980).
35. L. VOLPE AND M. BOUDART, *J. Solid State Chem.* **59**, 332 (1985).
36. W. THÖNI, P. GAI, AND P. B. HIRSCH, *J. Less-Common Met.* **54**, 263 (1977).
37. P. L. GAI AND P. A. LABUN, *J. Catal.* **94**, 79 (1985).
38. P. L. GAI, *Philos. Mag. A* **43**, 841 (1981).
39. J. M. DOMÍNGUEZ-ESQUIVEL, O. GUZMÁN-MAN-
DUJANO, AND A. GARCÍA-BÓRQUEZ, *J. Catal.* **103**,
200 (1987).